# Hydrodynamics of a Dual Fluidized Bed Gasifier. Part II: Simulation of Solid Circulation Rate, Pressure Loop and Stability

Kaiser, S.; Löffler, G.; Bosch, K.; Hofbauer, H.

Keywords: dual fluidized bed, pressure loop, modeling, stability, solid circulation, CFB

**Abstract**

This paper focuses on the determination of the solid circulation of a CFB gasification system with a dual fluidized bed concept and the distribution of the solid hold up at different fluidization conditions. A mathematical model of the riser was designed and implemented in a model of a dual fluidized bed system. This model contains routines for calculation of each section of the dual fluidized bed system. The behavior of the system was analyzed regarding changes in solid inventory and variations of geometry. A diagram is presented which allows an illustration of the influence of changes in the dual fluidized bed system configuration on the resulting stable operation points. Analysis concerning the effect of counter pressure on combustion and gasification side revealing the role of the seal loop in stabilizing the operation of the gasification system.

## 1. Introduction

A dual fluidized bed system allows the treatment of separated gas streams with the same circulating solid. Various applications such as adsorption processes and catalytic cracking can be found [1]. At Vienna University of Technology, a dual fluidized bed system for steam gasification was designed and tested during the last five years [2]. This gasification concept allows to produce high grade product gas (LHV 10 - 14 $MJ/m^3_s$). Gasification reactions take place in a bubbling fluidized bed. Remaining char is carried with the circulating bed-material into the combustion zone. Char and additional fuel for temperature control is burned in the combustion zone, operating at turbulent flow-regime. The heated bed-material is separated from the gas e.g. in a cyclone and transferred back to the gasification zone. This concept is also illustrated in Fig. 1. The hot bed-material supports the endothermic gasification reactions with heat. The solid circulation rate between gasification and combustion zone is necessary for heat supply of gasification reactions. The higher the solid circulation rate, the lower the temperature difference between gasification and combustion zone . Moreover, higher solid flux between the fluidized beds conveys more char from the gasification to the combustion zone, which reduces the required amount of additional fuel [3], [4]. To study the operation behavior as well as for detail engineering purpose a numerical model for predicting the solid circulation and the mass distribution of solids in both fluidized beds was designed and evaluated with data retrieved from a cold flow model.

Only few work of CFB loop predictions can be found in literature. Breault et. al. [5] analyzed a high velocity loop fluidized bed. Furthermore, the solid inventory of the system was not taken into account due to its open structure. Bai et.al. [6] analyzed a dual fluidized bed system with two risers, downcomers and two valves. The authors

showed a dominant influence of solids inventory, superficial gas velocities and the opening of the solids valves. Lei et. al. [7] had also shown the influence of solid inventory on CFB operation. They observed especially the behavior of a CFB furnance with and without valve. Both configurations differ from the dual fluidized bed system because of the implemented seal loop after the separator (refer Fig. 1) which is necessary for avoiding the gas mixing from gasification and combustion zone. Fluidized bed systems with valves differ from these without valves. The valve is used to control the solids circulation rate nearly independent of the pressure drop in the riser while in circulating fluidized bed systems without valve the pressure drop and the solid circulation rate are strongly linked. Kehlenbeck et al. [8] studied a fluidization system similar to that used in this work. He investigated the solid circulation rate in a cold flow model and found a dimensionless number to predict solid circulation depending on solid inventory, fluidization conditions and particle properties.

To study the stability of operation, the pressure profile of the circulation loop and the solid circulation rate a numerical model considering each section of the dual fluidized bed system was designed. Evaluation of the model is done with experimental data obtained at a cold flow model.

## 2. Experimental

Experiments were done in a perspex cold flow model with air at ambient conditions as fluidization agent for all sections of the dual fluidized bed system. The dimensions of the cold flow model and properties of used solid were calculated by downscaling an industrial sized power plant (8 $MW_{th}$) applying scaling criteria of Glicksman, et. al.

[9]. A summary of property data and dimensions of the cold flow model is given in Table 1.

Table 1: Data of cold flow model and industrial sized plant

| | cold flow model | industrial sized plant | unit |
|---|---|---|---|
| $D_{GAS,BOT}$ | 0.250 | ca. 1 | m |
| $D_{GAS,TOP}$ | 0.55 | ca. 2.5 | m |
| $D_{RIS}$ | 0.175 | ca. 0.85 | m |
| $h_{RIS}$ | 2.0 | ca. 9.7 | m |
| bed-material | bronze | quartz | |
| $d_s$ | 119 | 540 | µm |
| $\rho_s$ | 8750 | 2500 | $kg \cdot m^{-3}$ |
| $\rho_G$ | 1.28 | 0.3 | $kg \cdot m^{-3}$ |

Experiments were carried out by varying the fluidization of the riser according to

Table 2. The total mass flow of air was varied as well as the air staging at the bottom, primary and secondary gas inlets. Additional variations were done with the solid inventory of the fluidized bed system and the geometry of the connection between stationary bed and the riser. Further, it was shown, that the influence of fluidization of the gasification part on solid flux between the fluidized beds is negligible, therefore, it was held constant. Fluidization of seal loop and connection were also kept constant at minimum fluidization, because it was shown that they are fluidized at minimum fluidization conditions to minimize gas requirement and product gas dilution.

Table 2: Variations carried out in experiments

| | | |
|---|---|---|
| S/T | 0.15 - 0.5 | - |
| $Q_{BOT}$ | 0.0055 - 0.016 | $m^3_s \cdot s^{-1}$ |
| $Q_{GAS}$ | 0.014 | $m^3_s \cdot s^{-1}$ |
| $U_{RIS,TOP}$ | 2.9 - 4.6 | $m \cdot s^{-1}$ |
| $m_{SYS}$ | 105 - 130 | kg |

The experiments were carried out by measuring the pressure profile in each section of the cold flow model shown in Fig. 1 as well as the solid circulation rate. The realization of these measurements is described in Löffler et.al. [11].

## 3. Description of the model

The model was implemented into a FORTRAN90-code, with geometry, fluidization conditions and particle properties as input parameters. Each section of the model - combustion zone, gasification zone, separator, connection and seal loop are calculated iteratively shown in Fig. 2. The iteration is done until the pressure loop is closed.

### 3.1. Riser

The combustion zone of the gasification system operates at turbulent fluidization conditions. A dense zone, splash zone and dilute zone were considered in calculation. Main assumptions of the model are given in Table 3, a more comprehensive description of the model and fluidization conditions is given in [11].

Table 3: Assumptions of the riser model

| | |
|---|---|
| dense zone | modified two phase theory |
| splash zone | exponential decay of solid concentration |
| dilute zone | core-annulus model |
| $u_T$ | according to Richardson and Zaki [12] |
| $u_S$ | force balance |
| $u_a$ | 1 $m \cdot s^{-1}$ |
| $\varepsilon_a$ | $\varepsilon_{mf}$ |
| $\Delta p_{FR}$ | in transport zone according to Capes and Nakamura [13] |
| $\Delta p_{dyn}$ | no local consideration, but equally distributed overall dynamic pressure drop |

### 3.2. Gasifier

Gasification zone is designed to be in bubbling fluidization regime. The flow division in bubble and emulsion phase is described by the modified two-phase theory. Toomey and Johnstone [14] assumed that by increasing the gas velocity above the minimum fluidization velocity, the emulsion phase remains at minimum fluidization conditions and all gas in excess flows through the bubble phase. The actual visible bubble gas flow $Q_b$ is overestimated by the two-phase theory (e.g. Grace and Clift, [15]). The deviations are described by the correction factor Y.

$$Q_b = Y \cdot (U - U_{mf}) \cdot A \qquad (1)$$

Assuming the bubbles free of solids, the average bed voidage of the dense zone can be calculated as follows

$$\varepsilon_{GAS} = \delta_b + (1-\delta_b)\cdot\varepsilon_{mf} \tag{2}$$

where the voidage at minimum fluidization conditions can be calculated from the Ergun equation

$$\varepsilon_{mf}^3 + \frac{150\cdot \mathrm{Re}_{mf}}{\varphi^2\cdot Ar}\cdot\varepsilon_{mf} - \frac{150\cdot \mathrm{Re}_{mf} + 1.75\cdot \mathrm{Re}_{mf}^2\cdot\varphi}{\varphi^2\cdot Ar} = 0 \tag{3}$$

with Reynolds number according to Grace [16]

$$\mathrm{Re}_{mf} = \sqrt{27.2^2 - 0.0408\cdot Ar} - 27.2 \tag{4}$$

In literature a lot of correlations for the correction factor *Y* are given. Johnsson et al. [17] supposed following equation based on data of bed expansion in a 16 $MW_{th}$ stationary fluidized bed combustor

$$Y = \frac{0.26 + 0.7\cdot\exp(-3.3\cdot d_s)}{(0.15 + U - U_{mf})^{0.33}}\cdot\left(h + 4\cdot\sqrt{A_0}\right)^{0.4} \tag{5}$$

applying the correlation of Darton et al. [18] for the bubble growth, the single bubble velocity $v_{b,\infty}$, and providing that the bubble fraction $\delta_b$ and thus the average bed voidage is constant within the entire bed. This results in

$$\delta_b = \frac{1}{1 + \frac{1.3 \cdot (0.15 + U - U_{mf})^{0.33}}{0.26 + 0{,}7 \cdot e^{-3.3 \cdot d_p}} \cdot (U - U_{mf})^{-0{,}8}} \quad (6)$$

The gasifier was divided into discrete cells with height $h_{GAS,i}$. The pressure drop of each cell i of the bubbling fluidized bed is determined assuming solid acceleration and deceleration compensating each other and neglecting wall friction forces.

$$\Delta p_{GAS,i} = (1 - \varepsilon_{GAS,i}) \cdot \rho_s \cdot h_{GAS,i} \cdot g \quad (7)$$

The mass of solids in the bubbling fluidized bed can be calculated according to

$$m_{GAS} = \sum_i (1 - \varepsilon_{GAS,i}) \cdot \rho_a \cdot h_{GAS,i} \cdot A_{GAS,i} \quad (8)$$

### 3.3. Connection

The connection between gasification zone and combustion zone is realized as a fluidized inclined channel. The main task is to prevent the gas slip between gasification zone and the combustion zone without influencing the solid circulation. Excess fluidization agent in the connection must be avoided to minimize the dilution of product gas in the gasification zone. Moreover, it was shown in experiments, that large gas bubbles due to excess of fluidization agent block solid circulation by reducing the free cross-section area accessible for solid flow.

The pressure drop is a result of static pressure drop and solid-wall friction.

$$\Delta p_{CON} = \Delta p_{CON,hyd} - \Delta p_{CON,FR} \tag{9}$$

The static pressure drop can be determined using the equation

$$\Delta p_{CON,hyd} = g \cdot \rho_S \cdot (1-\varepsilon_{CON}) \cdot l_{CON} \cdot \sin\beta \tag{10}$$

For determination of the pressure drop due to wall friction, a lot of correlations exist in literature. The general structure of these correlations is given in equation (11):

$$\Delta p_{CON,FR} = \lambda \cdot \frac{u_{S,CON}^2}{2} \cdot \frac{A_{wall}}{A_{cross\,sec}} \cdot \rho_S \cdot (1-\varepsilon_{CON}) \tag{11}$$

Venderbosch, et.al. [19] gives a good overview about correlations for solid-wall friction coefficients $\lambda$ in fast fluidized beds but the obtained pressure drops differ in a wide range. Hofbauer [20] measured the solid-wall friction coefficient of an internally circulating fluidized bed and showed, that $\lambda$ depends strongly on the particle size. Larger particles cause higher solid-wall friction coefficients.

For the friction factor $\lambda$ depending on used materials, shape and size, no general correlation could be found for quantifying the friction coefficient. Hence, the correlation for $\lambda$ was determined using the results obtained from the experiments. In analogy to laminar flow of fluids, an equation of the type

$$\lambda = \frac{k_{CON}}{u_{S,CON}} \tag{12}$$

was chosen [19]. As it can be seen in Fig. 3 reasonable agreement to the experimental values can be obtained for the coefficient $k_{CON}$ of 3.5. The mass of solids in the connection can be calculated similar to equation (8).

### 3.4. Cyclone

The pressure drop between the top of the riser and the ambient pressure was estimated using an empirical correlation from Perry, et.al. [21].

$$\Delta p_{CYC,G} = k_{CYC} \cdot \rho_G \cdot U_G^2 \tag{13}$$

The parameter $k_{CYC}$ is mainly depending on cyclone geometry and was assumed to be 30 based on cold flow model measurements.

### 3.5. Seal Loop

The main task of the seal loop is to avoid gas mixing of combustion air with product gas. The downcomer and the standpipe of the seal loop are modeled as bubbling fluidized beds according to equations (2), (6) and (7).

The horizontal connection between these parts is modeled by using the same correlation for friction force as proposed for the connection part. The height of the bed at the side of the stationary fluidized zone is as high as the standpipe. The height

of the bed at the side of the combustion zone was calculated to fulfill the pressure balance of the seal loop

$$p_{OUT,RIS} - p_{OUT,GAS} = \Delta p_{SL,STA} - \Delta p_{SL,DOW} - \Delta p_{SL,HOR} \quad (14)$$

The mass of bed-material in the seal loop can be calculated according to (8).

### 3.6. Solids Jet

The solid jet from the standpipe of the seal loop into the bubbling fluidized bed has a negligible influence on the pressure drop. Nevertheless the mass of solids in the jet has to be determined according to

$$m_{JET} = h_{JET} \cdot \frac{G_S \cdot A_{RIS}}{u_T \cdot \varepsilon_{mf}^{n-1}} \cdot \frac{1-\varepsilon_{mf}}{\varepsilon_{mf}} \quad (15)$$

with $u_T$ as terminal velocity of the single particle and n as the Richardson-Zaki coefficient. The height $h_{JET}$ of the jet is calculated as the difference of the height level of the standpipe and the height of the bed of the bubbling fluidized bed in gasification zone.

### 3.7. Closing Pressure Loop and Mass balance

As can be seen in Fig. 2, the solid mass balance of the dual fluidized bed system is fulfilled by calculating the mass of bed-material in the gasification zone from

$$m_{GAS} = m_{SYS} - (m_{CON} + m_{RIS} + m_{CYC} + m_{SL} + m_{JET}) \quad (16)$$

The height of the stationary bed in the gasification zone is calculated until the mass of solid according to (16) is reached.

The pressure balance is solved by calculating the pressure drop of the riser iteratively (see also Fig. 2), until equation (17) is fulfilled.

$$p_{OUT,RIS} - p_{OUT,GAS} = \Delta p_{GAS} + \Delta p_{CON} - \Delta p_{RIS} - \Delta p_{CYC} \quad (17)$$

Table 4: Summary of assumptions of each part of the dual fluidized bed system

| | combustion zone | gasification zone | seal loop | connection | cyclone | jet |
|---|---|---|---|---|---|---|
| $\varepsilon$ | core-annulus model | emulsion: $\varepsilon_{mf}$ $\delta_b$ acc. (6) | emulsion: $\varepsilon_{mf}$ $\delta_b$ acc. (6) | $\varepsilon_{mf}$ | $\varepsilon_{RIS,OUT}$ | $\varepsilon_{mf}$ |
| $\Delta p_{DYN}$ | equally distributed | - | - | - | - | - |
| $\Delta p_{FRI}$ | acc. [13] | - | acc. (11) with $k_{CON}$=3.5 | acc. eqn. (11) with $k_{CON}$=3.5 | acc. eqn. (13) with $k_{CYC}$=30 | - |

## 4. Discussion

### 4.1. Pressure Profile

Fig. 4a shows the calculated and the experimental pressure profile of the fluidized bed system. The pressure profile of the riser, especially the influence of air staging and the diffuser, is discussed more comprehensively in [11]. The experimental value

at the highest position (height level of 2.2 m) was measured in the gas stream leaving the cyclone. As this point is insignificant for the circulation loop of the solids, it was not calculated. It can be seen, that the connections between gasification zone and combustion zone are operating at a higher pressure level to avoid gas mixing between this zones.

Fig. 4b shows the pressure profile at a higher ratio of secondary air in the riser, resulting in a lower solid circulation rate. At the height level of 0 - 0.2 m two conspicuous differences to Fig. 4a can be observed. Higher solid circulation rates cause an increased resistance due to the increased solid-wall friction in the seal loop and the connection (refer to equation (9)). Thus, the bed inventory is shifted into the stationary bed decreasing the pressure drop of the riser with increasing solid circulation rate.

### 4.2. Analysis of operation behavior

To analyze the system's behavior, it is necessary to elaborate on the interaction between riser and the entire fluidized bed system. Fig. 5 illustrates the behavior of the riser and the entire system. The riser is calculated at constant fluidization conditions but different pressure drops. As expected, the higher the pressure drop, the higher gets the elutriation of solid from the riser [11] (e.g. Line A in Fig. 5). The entire dual fluidized bed system is examined at different solid circulation rates and constant geometry and solid inventory (e.g. Line B in Fig. 5).

It is shown, that higher solid circulation rate causes a displacement of solid mass from the riser to stationary gasification zone which is also illustrated by Fig. 6. This can be explained by the increase in pressure drop due to wall friction in the seal loop

and the connection at higher rates of solid circulation. This reduces the pressure drop of the connection, leading to an increase in the pressure drop of the stationary bubbling bed (refer equation (17)). In this way, the mass of solids in the gasification zone and the seal loop increase, reducing the mass in the riser according to equation (16). Thus, the closed loop system causes a decreasing pressure drop of the riser with higher solid circulation rate as shown for instance by Line B in Fig. 5.

Intersection points between riser-lines and system-lines show stable operation points of the dual fluidized bed system. These operation points are the calculation results of the model according to Fig. 2.

### 4.3. Changes in system inventory

Fig. 5 illustrates the influence of solids inventory on operational behavior of the dual fluidized bed system. At constant fluidization conditions, the stable operation points are shifted towards higher solid circulation rates, accompanied by increasing pressure drop of the riser. This effect can be explained by the extension of the dense zone of the riser due to higher solid inventory [11]. Fig. 6 shows the influence of the solid inventory on the distribution of solid mass between the riser and the stationary bed. The ratio of solid mass in the riser and the solid mass in the stationary bed decreases with higher solid inventory because of the larger square section of the stationary bed.

### 4.4. Changes in geometry

The cold flow model was designed with an inclination of the connection part of 30°. Experiments showed small solid circulation rates at smaller inclinations. With this

configuration all experiments were carried out. Similar to the behavior at different solid inventory a more inclined connection pushes more bed material in the riser, increasing the solid circulation (Fig. 7).

### 4.5. Stability at variations in outlet pressures

An important criterion for operating a dual fluidized bed system is the stability of solid circulation at changes in the outlet pressures. This can be caused in regular operation due to downstream fabric filters as well as at power plants malfunctions. As shown in Fig. 8, rising counter-pressure at the riser outlet reduces the solid circulation rate. The same effect can be observed for higher pressure drops of the cyclone. Therefore, an efficient separator design is important.

An increase of the outlet pressure on gasification side causes an increase in solid circulation rate because more bed material is pushed into the combustion zone.

Stability of solid circulation is mainly determined by the design of the seal loop as can be seen in Fig. 9. Counter-pressure at combustion side leads to a decrease of bed height in the downcomer. Operation is limited by the decrease of solid circulation rate or by the blowout of the seal loop. Counter-pressure at gasification leads to an increase of bed height in the downcomer. The operation limits are not as important as at counter pressure at riser outlet. Overflow of the downcomer could occur, on the other hand gas leakage due in the decrease of pressure drop of the connection between gasification and combustion zone could happen.

## 5. Evaluation of the model

In Fig. 5 the results obtained from the experiments are compared to the model results. It can be seen, that trends of pressure drop of the riser at different solid circulation rate are well described by the model. Nevertheless, the coherence of pressure drop and solid circulation rate differs from the measured results.

A comparison between calculated and measured solid circulation rates is given in Fig. 10. Above 50 $kg \cdot m^{-2} \cdot s^{-1}$ nearly all data points are lying within a deviation range of +/- 20%, which complies to the experimental accuracy for solid circulation rate. The deviation for the solid circulation rate below 50 $kg \cdot m^{-2} \cdot s^{-1}$ is due to the calculation of the splash zone [11]. Further investigations concerning measurements of the voidage profile in the bottom region of the riser are necessary, considering the air staging is necessary [11].

A sensitivity analysis of the parameters, which are estimated and fitted when applying the model is carried out according to Table 5. The sensitivity of the parameters are calculated according to

$$S = \frac{\Delta G_S / G_{S,S\,\mathrm{tan}\,dard}}{\Delta P / P_{S\,\mathrm{tan}\,dard}} \qquad (18)$$

Table 5: Sensitivity analysis for the model parameters (at $U_{RIS}$=4.2 $m \cdot s^{-1}$, S/T=0.15, B/T=0.18, Solid inventory 105kg)

| Parameter | Standard | Variation range | Sensitivity |
|---|---|---|---|
| $k_{CYC}$ | 30 | +/- 20% | 0.08 |
| $\lambda$ | $\frac{3.5}{u_S}$ | +/- 20% | 0.29 |
| $(1-\varepsilon_{CYC})$ | $(1-\varepsilon_{RIS,TOP})$ | +/- 20% | 0.02 |

The overview given in Table 5 confirms, that none of the assumed parameters shows a significant sensitivity on the predicted results of the model. The most sensitive parameters on the model are the decay constant a and the voidage above the transport disengaging height $\varepsilon_{\infty}$ of the riser, which are discussed in [11].

## 6. Conclusion and further work

A numerical model of a dual fluidized bed system was designed. Evaluation with experimental data shows sufficient accordance of the mathematical model regarding the solid circulation rate and the pressure profile within the system. The influence of the geometry of the connection between the stationary fluidized gasification zone and the riser as well as the influence of the solid inventory were investigated. Larger inclinations of the connection and high solids inventory lead to in higher solid circulation rates. To analyze these influences a method was presented to illustrate the interaction between riser and the entire fluidized bed system. Also it was shown, that higher solid circulation rates cause a displacement of solid holdup from the combustion zone to gasification zone. This method was also used for studying the influence of increasing pressure at outlet of the riser and gasification zone. An

increase in pressure at riser outlet reduces the solid circulation while an increase in pressure at outlet of the stationary bed shows an increase in the solids circulation rate. It was pointed out, that due to the seal loop a stable operation of the fluidized bed system can be achieved.

Further work will be done in observing the inclined connection between gasification and combustion part using different types of solids. Additionally, solid circulation rate measurements and pressure loop measurements on a 8 $MW_{th}$ demonstration plant in Guessing, Austria, are planned.

**Acknowledgments**

Financial support from the Austrian funds program "Knet" is gratefully acknowledged.

**List of Symbols**

| | | |
|---|---|---|
| a | decay constant of the riser | $[m^{-1}]$ |
| A | Area | $[m^2]$ |
| Ar | Archimedes number | $Ar = \frac{\rho_G \cdot (\rho_P - \rho_G) \cdot g \cdot d_P^3}{\eta^2}$ |
| B/T | ratio of bottom air to total air into riser | |
| D | Diameter | [m] |
| dP | particle diameter | [m] |
| $G_S$ | solid circulation rate, related to top of the riser | $[kg \cdot m^{-2} \cdot s^{-1}]$ |
| g | gravitational acceleration | $[m \cdot s^{-2}]$ |
| h | height | [m] |

| | | |
|---|---|---|
| $k_{CYC}$ | parameter for cyclone | $[s \cdot m^{-1}]$ |
| $k_{CON}$ | parameter for connection part | [1] |
| m | mass | [kg] |
| n | Richardson Zaki coeff. | [1] |
| p | pressure | [Pa] |
| P | Parameter, general | |
| Q | Volume flow | $[m^3 \cdot s^{-1}]$ |
| Re | Reynolds number | $Re = \frac{\rho \cdot U \cdot d_P}{\eta}$ |
| S/T | ratio of secondary air to total air into riser | |
| u | velocity | $[m \cdot s^{-1}]$ |
| $u_T$ | terminal velocity | $[m \cdot s^{-1}]$ |
| U | superficial velocity | $[m \cdot s^{-1}]$ |

*Greek letters*

| | | |
|---|---|---|
| $\propto$ | above transport disengaging height | |
| $\beta$ | inclination | [°] |
| $\delta_b$ | bubble fraction | [1] |
| $\Delta p$ | pressure drop | [Pa] |
| $\varepsilon$ | voidage | [1] |
| $\eta$ | dyn. Viscosity | $[kg \cdot m^{-1} \cdot s^{-1}]$ |
| $\varphi$ | sphericity | [1] |
| $\lambda$ | friction coefficient | [1] |
| $\rho$ | Density | $[kg \cdot m^{-3}]$ |

*Indices*

| | |
|---|---|
| a | annulus |
| b | bubble phase |
| BOT | bottom gas inlet |
| CON | connection between gasification and combustion zone |
| CYC | cyclone |
| DOW | downcomer |
| dyn | dynamic |
| FR | friction |
| g | gas |
| GAS | gasification zone (bubbling regime) |
| hyd | hydrostatic |
| hor | horizontal |
| JET | solid jet from seal loop into stationary bed |
| mf | minimum fluidization |
| PRI | primary gas inlet |
| RIS | riser, combustion zone |
| s | solid |
| SEC | secondary gas inlet |
| SL | seal loop |
| STA | standpipe |
| SYS | entire dual fluidized bed system |
| TOP | at the top of |
| TOL | tolerance |

## References


[1] H. Hofbauer: Internally Circulating Fluidized Beds, Fundamental and Applications; Proc. of the 1st SCEJ Symposion on Fluidization, Tokyo, 1995, 275.

[2] E. Fercher, H. Hofbauer; T. Fleck; R. Rauch; G. Veronik: Two Years Experience with the FICFB-Gasification Process, 10th European Conference and Technology Exhibition, Würzburg, Jun e 1998

[3] S. Kaiser, K. Weigl, Ch. Aichernig; A. Friedl, H. Hofbauer: Simulation of a highly efficient dual fluidized bed gasification process, 3rd European Congress on Chemical Engineering, Nürnberg, June 2001

[4] S. Kaiser, K. Weigl, G. Schuster, H. Tremmel, A. Friedl, H. Hofbauer, 1st World Conference and Exhibition on Biomass for Energy and Industry, Sevilla, June 2000

[5] R.W. Breault, V.K. Mathur: High Velocity Fluidized Bed Hydrodynamic Modeling. 1. Fundamental Studies of Pressure Drop, Ind. Eng. Chem. Res., 28 (1989) 684

[6] D. Bai, A.S. Issangya, J.-X. Zhu, J.R. Grace: Analysis of the Overall Pressure Balance around a High-Density Circulating Fluidised Bed, Ind. Eng. Chem. Res. 36 (1997) 3898

[7] H. Lei, M. Horio: A comprehensive pressure balance model of circulating fluidized beds, J. Chem. Eng. Jap. 31 (1998) 83

[8] R. Kehlenbeck, J. Yates, R. Di Felice, H. Hofbauer, R. Rauch: Novel Scaling Parameter for Circulating Fluidized Beds, AIChE J. 47 (2001) 582-589

[9] L.R. Glicksman: Scaling Relationships for Fluidized Beds, Chem. Eng. Sci. 39 (9) (1984) 1373-1379.

[10] K. Bosch, H. Hofbauer: Untersuchungen am Kaltmodell für das Projekt Biomasse Kraftwerk Güssing, internal report RENET 07/2000 (2000)

[11] G. Löffler, S. Kaiser, K. Bosch, H. Hofbauer: Hydrodynamics of a Dual Fluidized Bed Gasfier. Part I: Simulation of a Riser with Gas Addition and Diffuser, submitted to this journal (2001).

[12] J.F. Richardson, W.N. Zaki: Sedimentation and Fluidisation: Part 1, Trans. Instn Chem. Engrs 32 (1954) 35

[13] C.E. Capes; K. Nakamura: Vertical pneumatic conveying: an experimental study with particles in the intermediate and turbulent flow regimes, Can. J. Chem. Eng. 52 (1973) 31

[14] R.D. Toomey, H.F. Johnstone: Gaseos Fluidization of Solid Particles, Chem. Eng. Prog. 48 (1952) 220

[15] J.R. Grace, R. Clift: On the Two-Phase Theory of Fluidization, Chem. Eng. Sci. 29 (1974) 327

[16] J.R. Grace: Fluidized Bed Hydrodynamics, in Handbook of Multiphase Systems, G. Hetsroni (Ed.), Washington Hemisphere Publishing, Washington

[17] F. Johnsson, S. Andersson, B. Leckner: Expansion of a freely bubbling fluidised bed, Powder Tech. 68 (1991) 117

[18] R.C. Darton: A Bubble Growth Theory of Fluidized Bed Reactors, Trans. Instn Chem. Engrs. 57 (1979) 134

[19] R.H. Venderbosch; W. Prins, J.H.A. Kiel, W.P.M. Swaaij, Solids Hold-Up and pressure gradient in a small laboratory riser, Circulating Fluidized Bed Technology V, Bejing, May 1996

[20] H. Hofbauer: Experimentelle Untersuchung an einer zirkulierenden Wirbelschicht mit Zentralrohr, Ph. Thesis, Vienna University of Technology, 1982

[21] R. H. Perry: Perry's Chemical Engineers Handbook, 6th Ed.; McGraw Hill International Ed.; 1988

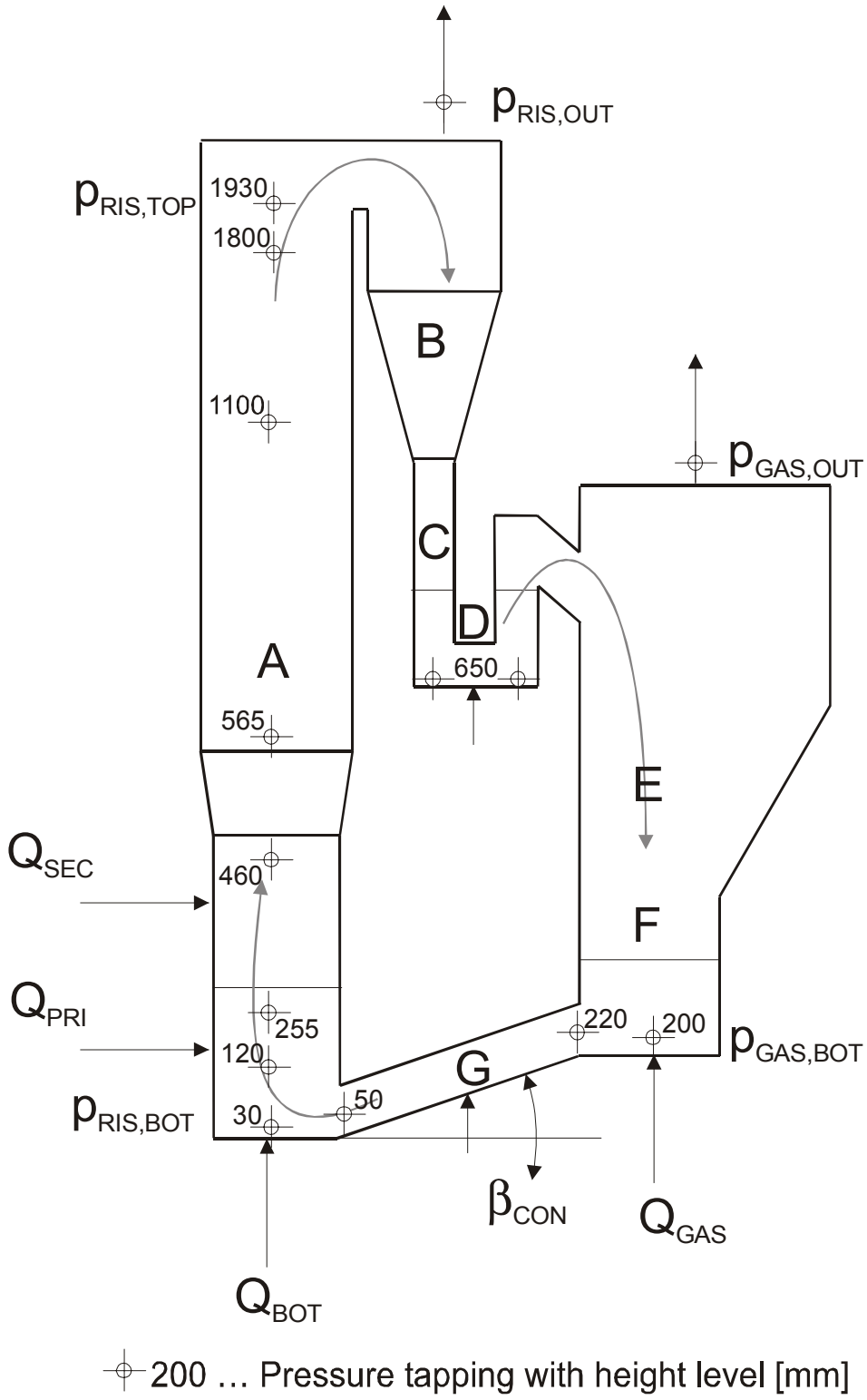


Fig. 1: Dual fluidized bed system with (A) riser (combustion zone), (B) separator, (C) downcomer, (D) seal loop, (E) solids jet, (F) bubbling fluidized bed (gasification zone), (G) connection

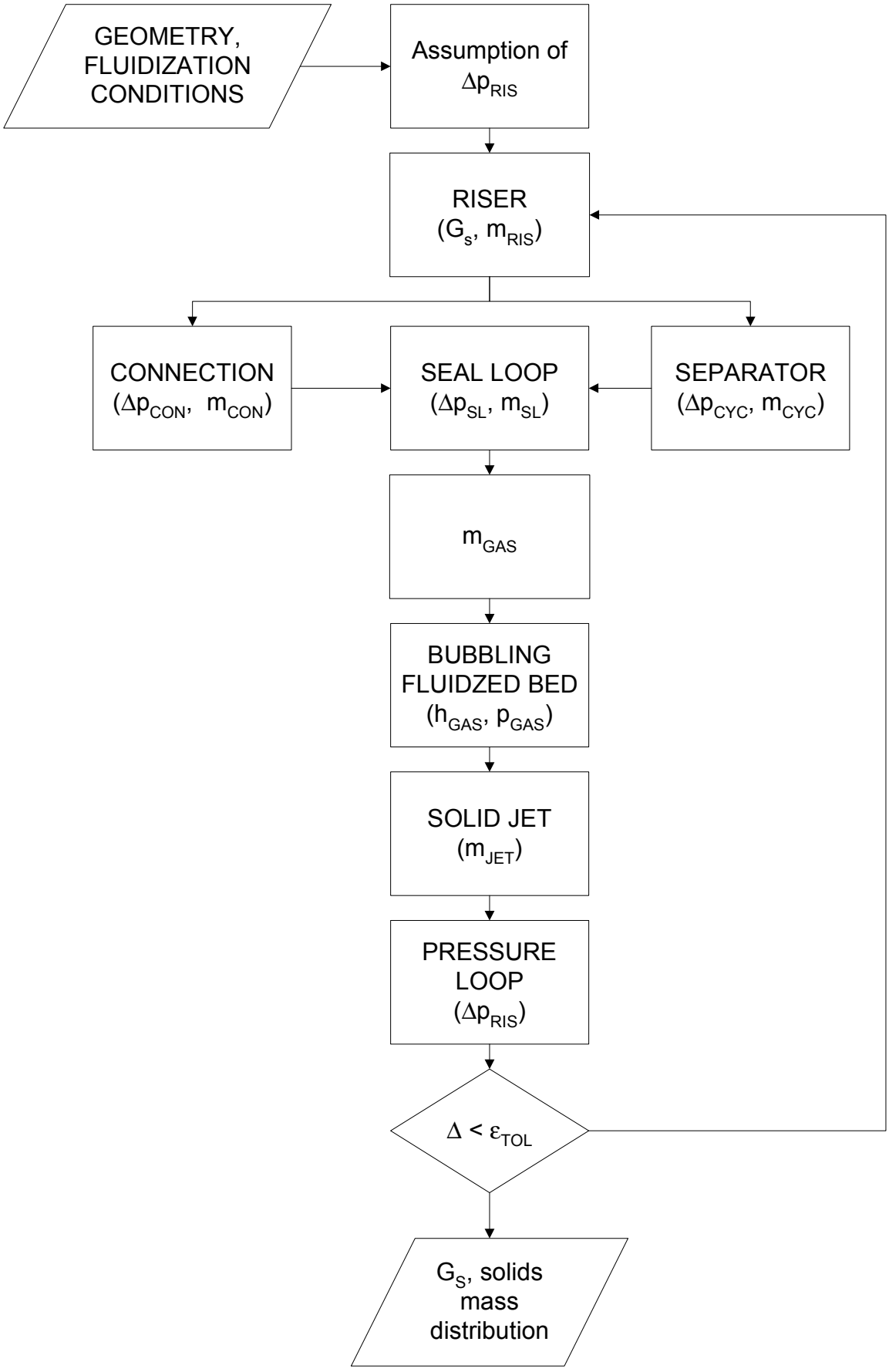


Fig. 2: Structure of pressure loop determination

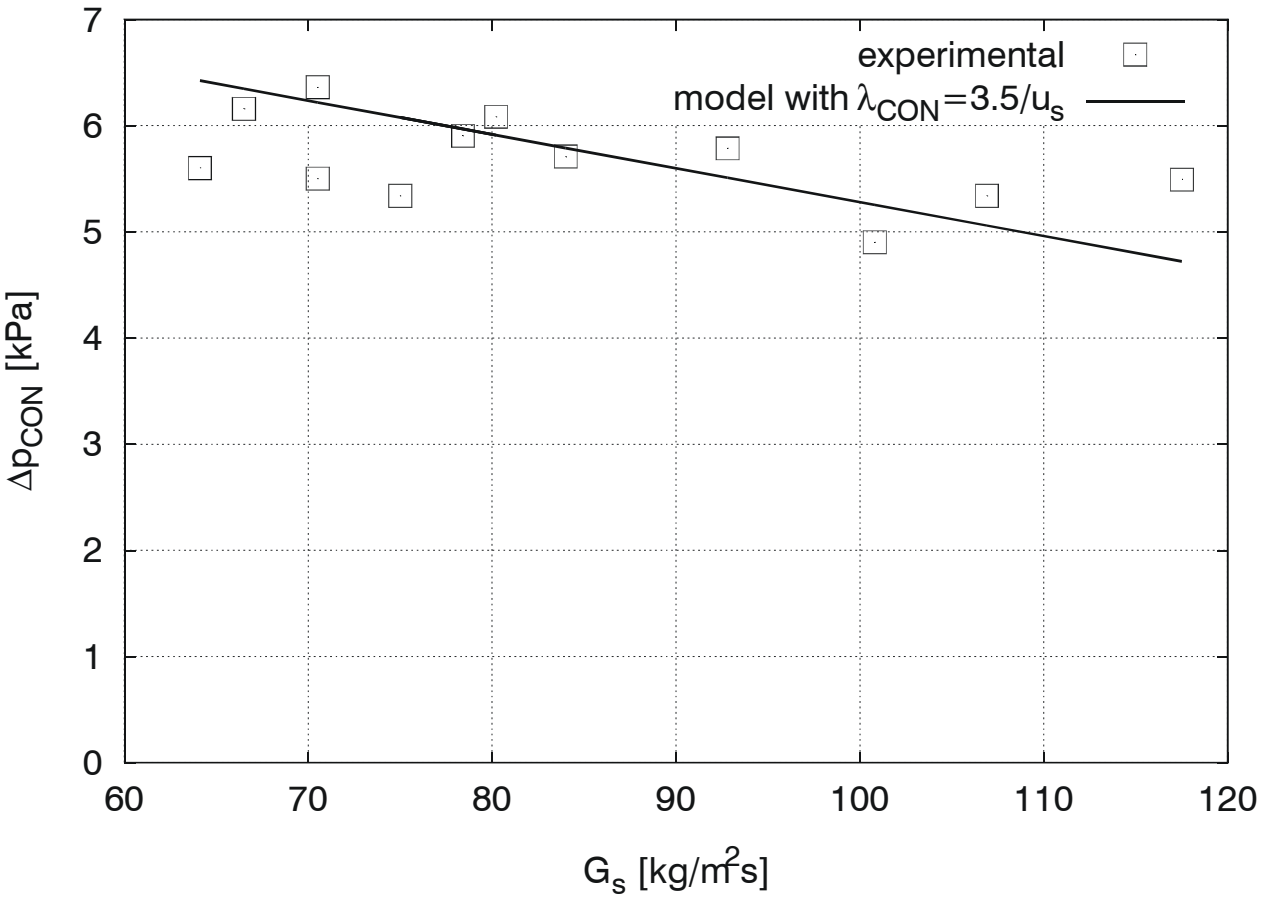


Fig. 3: Pressure drop over connection at different solid fluxes

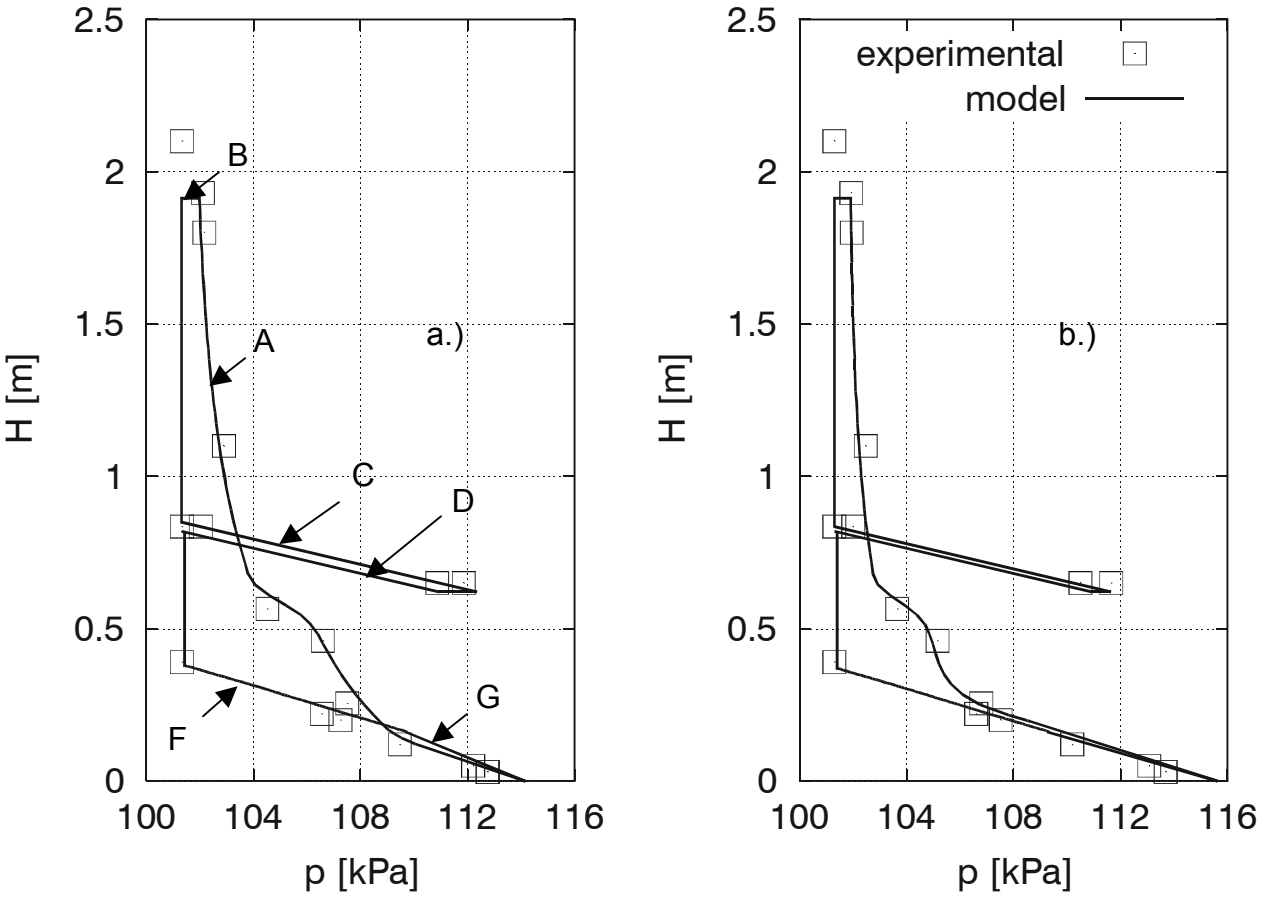


Fig. 4: Comparison of calculated pressure profile with experimental data (a) Solid inventory 105 kg, $U_{RIS}$=4.2 m·s$^{-1}$, S/T=0.15, B/T=0.18, $G_s$=117 kg·m$^{-1}$s$^{-2}$, (b) Solid inventory 105 kg, $U_{RIS}$=4.2 m·s$^{-1}$, S/T=0.5, B/T=0.06, $G_s$=66kg·m$^{-1}$s$^{-2}$ Letters in a.) refer to Fig. 1

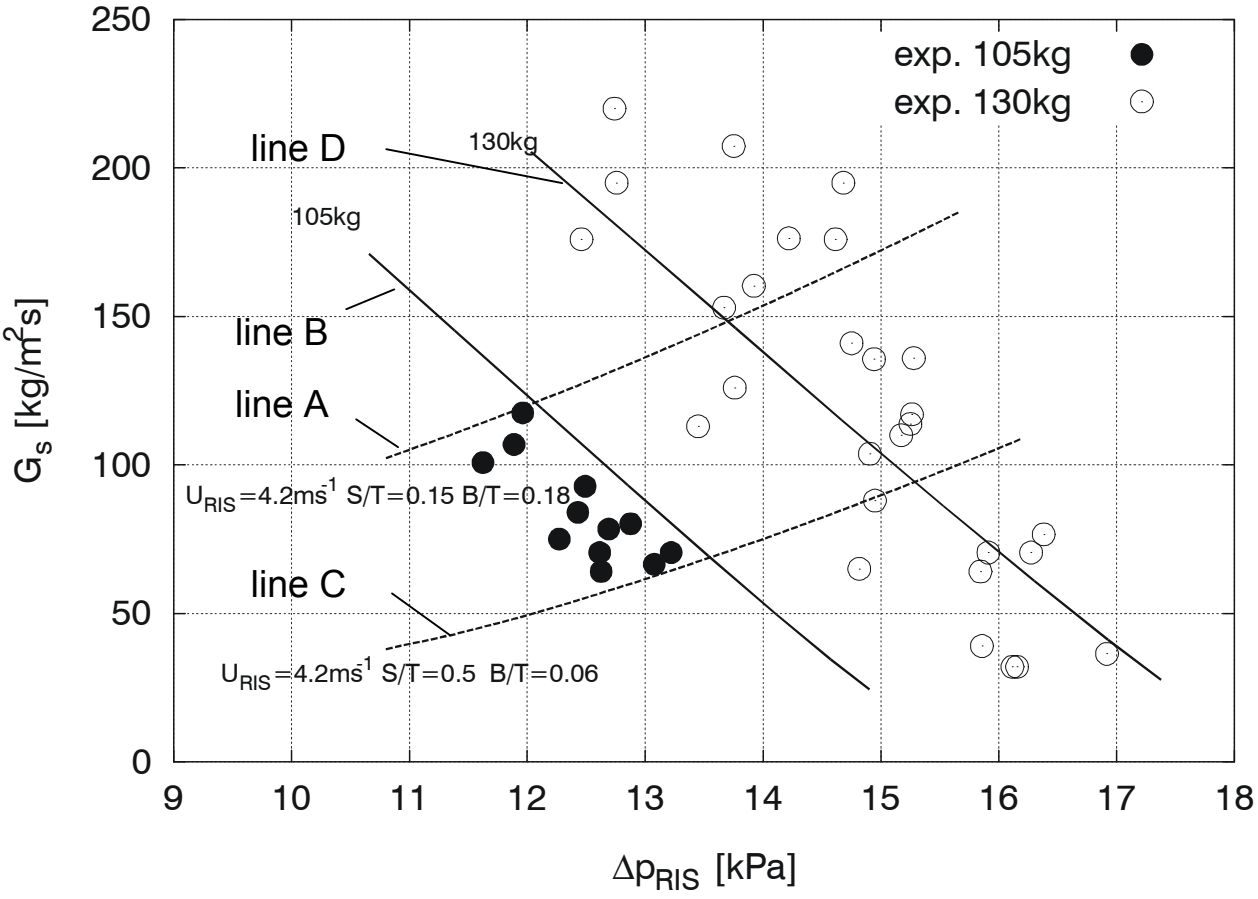


Fig. 5: System and riser behavior with experimental results. Line A and C belong to the riser while Line B and D belong to the whole fluidized bed system

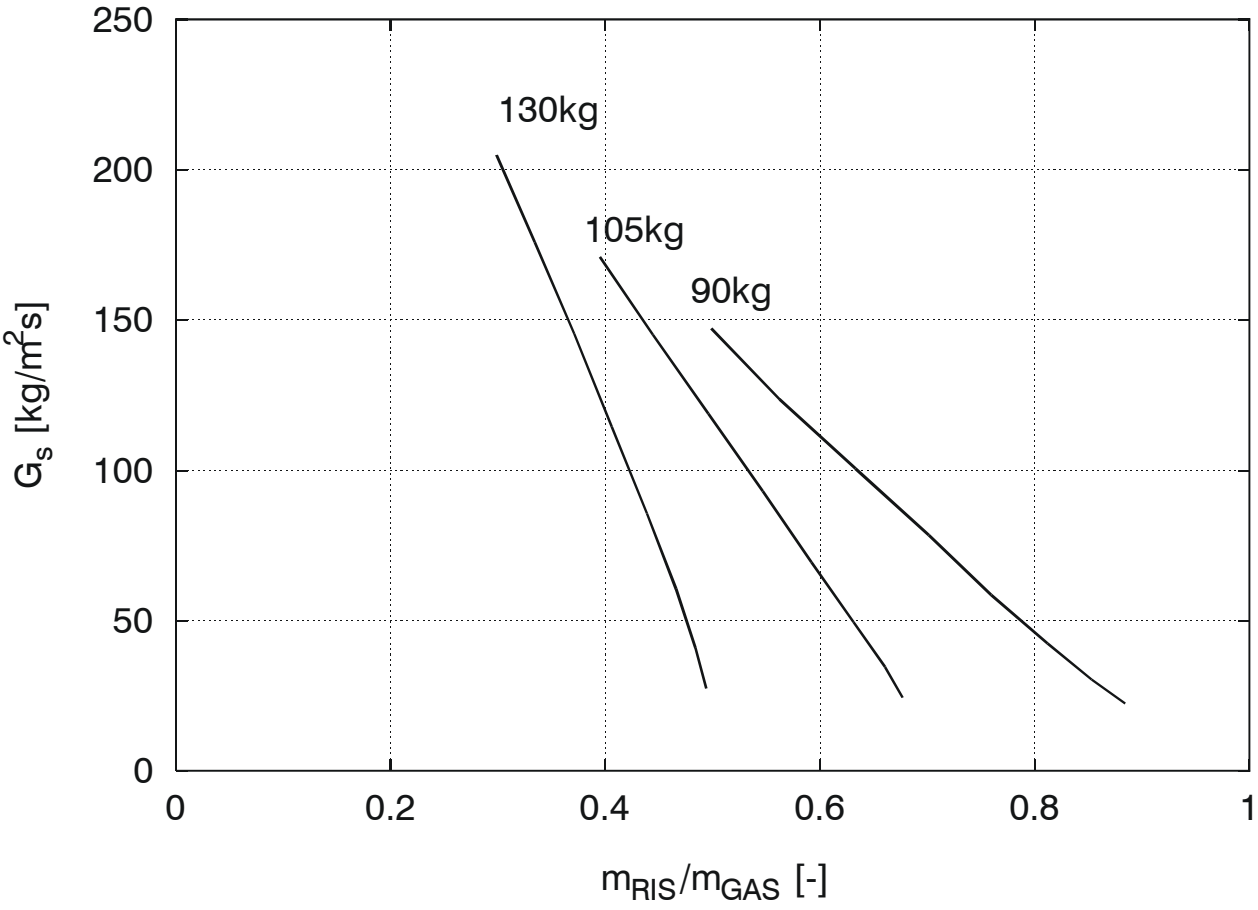


Fig. 6: Mass distribution between gasification and combustion zone

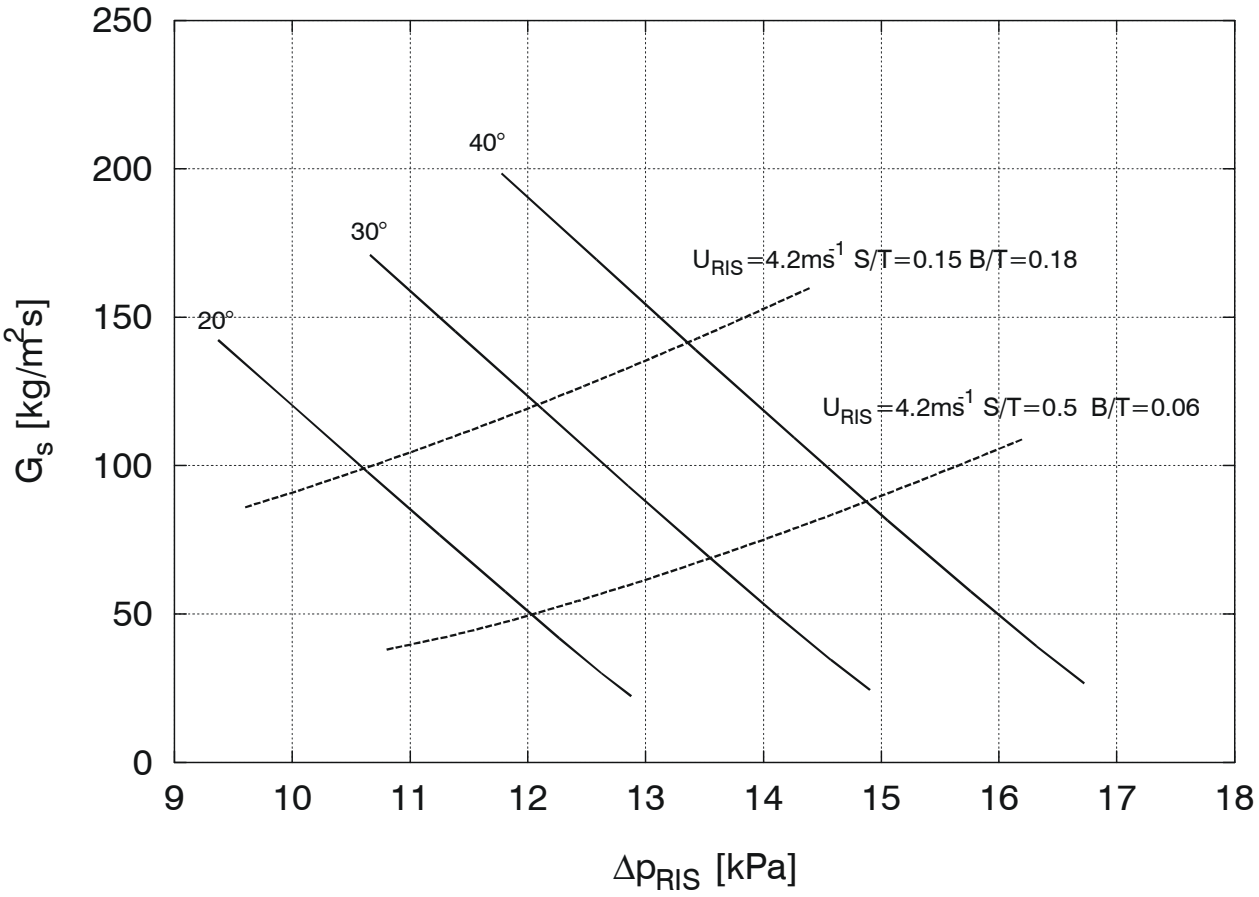


Fig. 7: Influence of connection inclination

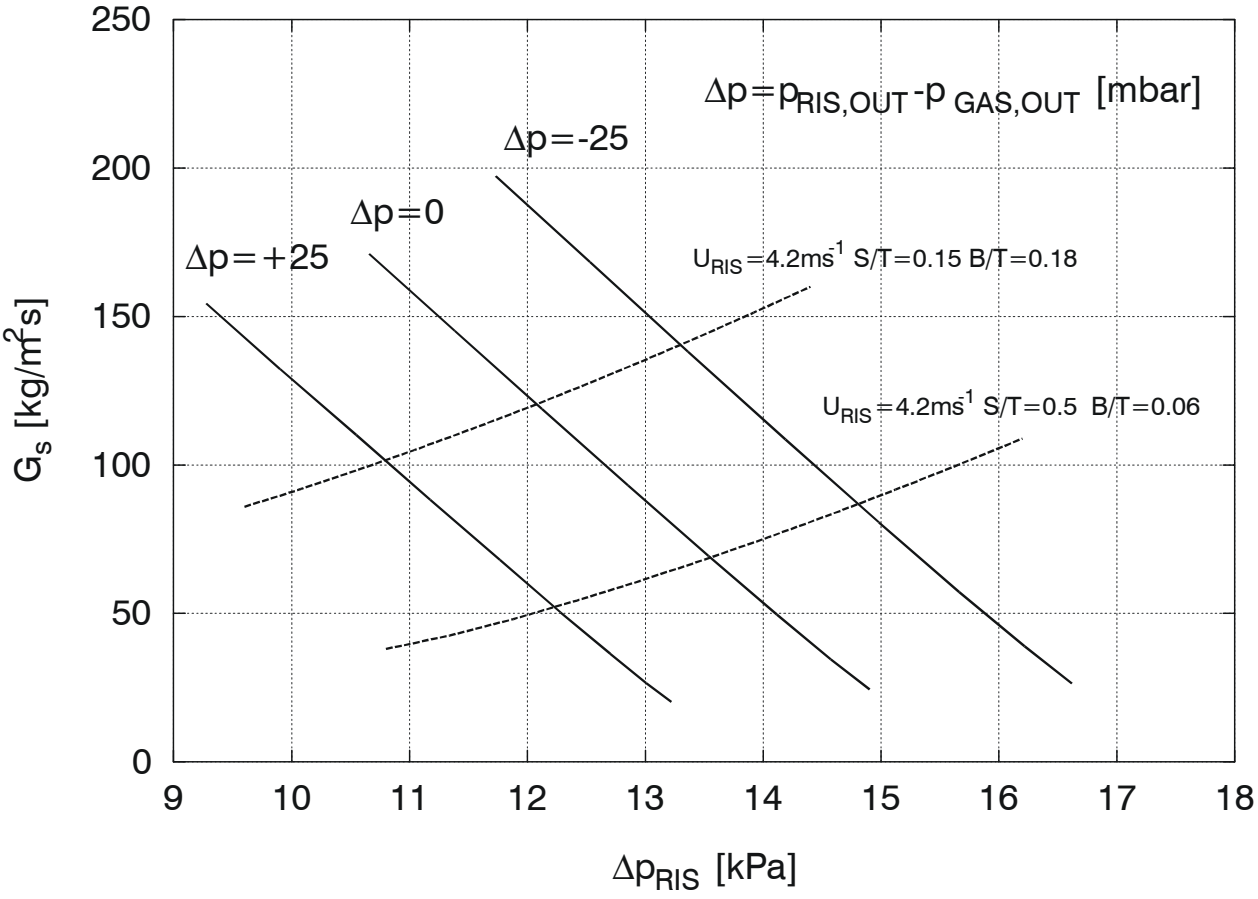


Fig. 8: Influence of counter-pressure on system behavior

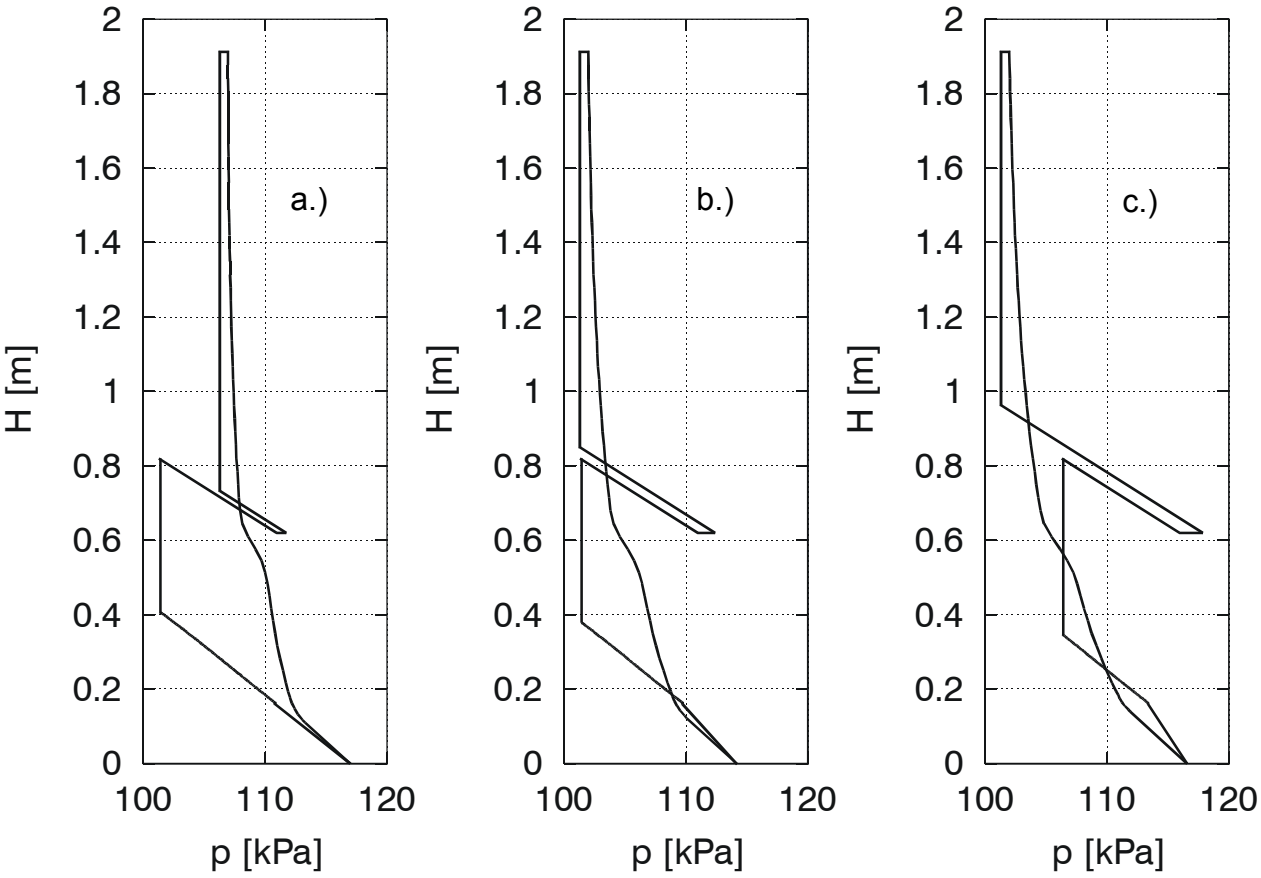


Fig. 9: Influence of pressure drop between gas outlet of combustion and gasification side with fluidization conditions remaining constant (a) 50 mbar counter-pressure on combustion side resulting in 62 $kgm^{-2}s^{-1}$, (b) equal pressure with 116 $kgm^{-2}s^{-1}$, (c) counter-pressure at gasification side of 50 mbar resulting in 155 $kgm^{-2}s^{-1}$

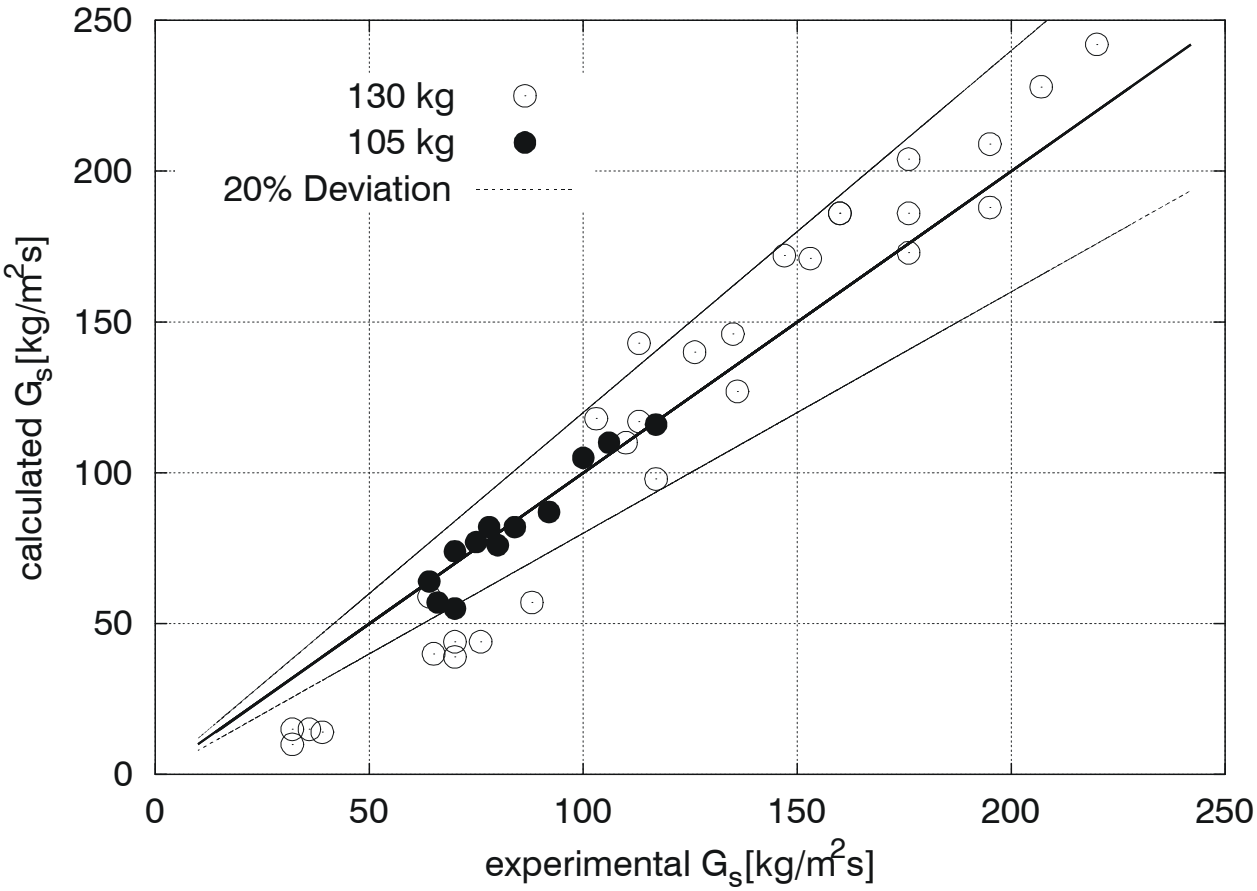


Fig. 10: Comparison of model with experimental data, obtained at different solid inventory